ATMOSPHERIC CORRECTION VALIDATION OF CASI IMAGES ACQUIRED OVER THE BOREAS SOUTHERN STUDY AREA*

N. T. O'NEILL, F. ZAGOLSKI, M. BERGERON, A. ROYER,
CARTEL, Université de Sherbrooke,
Sherbrooke (Québec),
CANADA, J1K-2R1.

J. R. MILLER,
Department of Physics and Astronomy,
York University,
Toronto (Ontario),
CANADA, M3J-3K1.

J. FREEMANTLE,
Earth Observations Laboratory,
Institute for Space and Terrestrial Science,
Toronto (Ontario),
CANADA, M3J-3K1.

ABSTRACT: High altitude atmospheric correction procedures for remotely sensed images acquired by the Compact Airborne Spectrographic Imager (CASI) during the Boreal Ecosystem-Atmosphere Study (BOREAS) were tested over a variety of validation sites. Regression analysis on multi-altitude CASI data was employed to estimate apparent surface Bidirectional Reflectance Factors (BRFs) which served as ground truth spectra for validating the atmospheric correction procedures. Absolute radiance calibrations of CASI data permitted normalized radiances to be input into a standard atmospheric correction package (a variant of the H5S model) for image transformation to apparent surface BRF. In addition, relative BRF calibrations derived from in-situ measurements of well-characterized multi-pixel sized calibration panels and ratios of upwelling CASI radiance signals normalized by downwelling CASI irradiance signals were employed to independently compute the multi-altitude apparent BRFs used in deducing the ground truth apparent BRF spectra. Assuming a knowledge of the local aerosol optical depth and some apriori information on the type of environment surrounding each validation site the average absolute differences between the uncorrected and corrected apparent BRFs and the ground truth apparent BRFs were 1.6% versus 0.6% respectively in the visible spectral region and 1.1% versus 1.1% respectively in the near infrared region. The errors in the corrected BRFs can be reduced at the expense of introducing increased complexity in the input parameter requirements of the atmospheric correction model.

* *Revised version returned to the Canadian Journal of Remote Sensing, July 2, 1997.*

INTRODUCTION

The success of the remote sensing component in the BOREAS experiment rests on the capability of providing georeferenced data bases from which relevant forest ecosystem parameters can be extracted at a temporal and spatial scale commensurate with the needs of the application teams. The spectral Bidirectional Reflectance Factor (BRF) of a given surface target is the most target-intrinsic optical parameter generated by remote sensing technology since it is in principle independent of sensor properties, atmospheric state and illumination intensity. The objective of the remote sensing teams in BOREAS was accordingly to provide BRF images with acceptable and well defined tolerances.

The extraction of apparent surface BRF spectra is non trivial since the atmosphere between the sensor and the target and between the solar source and the target is known to significantly modify the spectral signatures generated by the forest canopy. Such modifications are clearly unstable in time and hence preclude or seriously limit temporal studies of optically derived indicators of ecosystem state. Coupled with the bidirectional effects of the forest canopy the atmospheric effect also compromises bio-optical inversion algorithms which seek to retrieve pertinent biophysical indicators from image pixels whose BRF is acquired in a variety of illumination and viewing conditions. The literature is replete on the atmospheric corrections required to eliminate the effect from satellite and very high altitude airborne imagery (see Fraser et al., 1992; Kaufman and Tanré, 1993; Zagolski and Gastellu-Etchegorry, 1995, for example) while considerably less work has been realized for high to intermediate sensor altitudes (O'Neill et al., 1995).

The development of a surface BRF extraction methodology which is built upon sound instrumental calibration and field validation techniques as well as standard atmospheric correction models with pragmatic input data requirements is fundamental to the ultimate utility of remote sensing data. The objective of the present work was to analyze the accuracy of standard atmospheric corrections procedures for the estimation of surface BRF from calibrated high-altitude airborne BOREAS/CASI imagery and to validate such procedures using multi-altitude CASI imagery. In order to perform this analysis we have employed an adapted airborne version (CAM5S) of the 5S and 6S radiative transfer codes. Although these codes exist in various versions they represent a remote sensing standard which is used by a large part of the applications community.

The multi-altitude aspect of the airborne imagery will contribute first and foremost, a pragmatic and highly relevant form of "ground truthing" inasmuch as apparent (atmospherically influenced) BRFs acquired at each altitude can be extrapolated to the surface by semi-analytical means. This approach eliminates much of the inter-calibration and scale sampling problems associated with traditional ground based measurements and can be much more representative than the inevitable sparse point sampling limitations of the ground techniques. In addition these images and associated (downwelling and upwelling) irradiance information collected at the same spectral resolution as the images will provide optical information on the atmosphere which can be used to analyze and understand the atmospheric influences on the remotely sensed data (O'Neill et al., 1997) and hence to better understand the error budget in the atmospheric correction process. Furthermore this derived optical information as well as the estimated surface BRFs will provide data redundancy with respect to other airborne and satellite remote sensing projects carried out as part of BOREAS.

Finally, absolute calibration in radiance is the usual and accepted methodology for estimating apparent surface BRF. In this work we seek to demonstrate that in-situ BRF "calibration" using large at-surface calibration panels of known BRF characteristics and the ratio of at-sensor radiance to irradiance signals provides a complementary verification of calibration and correction technique as well as increasing confidence in the complete atmospheric correction methodology.

THEORETICAL BACKGROUND

Airborne Atmospheric Corrections

The greater part of the theoretical background and nomenclature needed to understand the atmospheric correction of apparent BRF images acquired by the CASI instrument is given in O'Neill et al. (1995). In this section and in the Appendix we present some additional considerations which are meant to complement the background presented in that paper in terms of surface BRF contributions and in order to provide a link with the 5S/6S code and documentation. The radiative transfer equations and parameters in the above reference and below are meant to be eithor monochromatic or band averaged in the spectral domain: for simplicity we have omitted spectral arguments or subscripts.

It is important to distinguish between two types of imagery metrics. The apparent BRF, which can be generated by the CASI sensor, is expressed as:

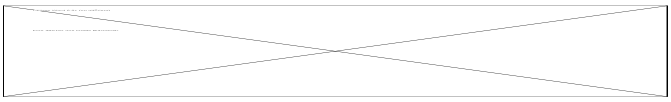

where τ_g refers to the atmospheric optical depth from ground level to the sensor, $L(\tau_g, \mu, \phi)$ is the at-sensor radiance and E_{tot} (τ_g, μ_o, ρ) is the downwelling irradiance at the sensor. ρ is the bi-hemispherical reflectance averaged over the total ground surface (see the glossary for a complete list of definitions). What we will call the normalized radiance and which is often referred to as the apparent reflectance in the literature associated with the 5S and 6S codes is given by:

where E_o is the exo-atmospheric solar beam irradiance. These two monochromatic metrics ((1a) and (1b)) are related by the expression:

If (as is usually done) the non-Lambertian multiple reflection effects between the atmosphere and the surface on the downwelling irradiance are ignored then the downwelling irradiance may be written as:

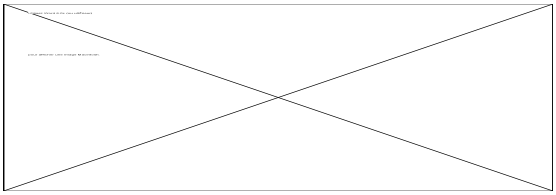

where $\rho(\tau_g)$ is an estimate of the bi-hemispherical reflectance at the top of the layer of optical thickness τ_g and $s(\tau_g)$ is the spherical albedo for the optical layer above the sensor. T_{tot} represents the standard 5S/6S total (direct plus diffuse) transmission for the optical layer above the sensor.

The details of the expansion of the normalized radiance and the apparent BRF in terms of the various components are given in the Appendix. The essential paradigm for atmospheric corrections can be expressed as a single equation:

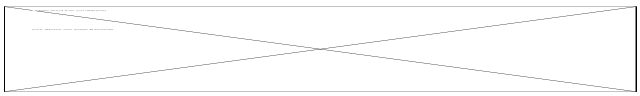

for normalized radiance and:

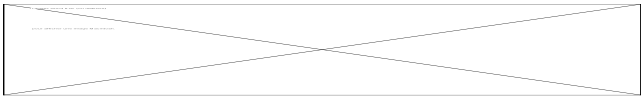

in terms of apparent BRF. The angular dependencies inherent in such expressions have, for the sake of simplicity, been suppressed. The subscripts "sur", "env" and "atm" represent respectively the surface target, the environment (pixels other than the target pixel) and the pure atmospheric contribution. The parameter $h(\tau_g)$, defined in the Appendix, represents the transmission of total irradiance from the aircraft to the ground.

Extraction of Apparent Surface BRF and Atmospheric Optical Parameters From Multi-Altitude apparent BRF data

The processing of multi-altitude images for atmospheric correction validation should include a physically-coherent multi-altitude regression capability for simultaneously extrapolating the BRF images to zero altitude. This method, in addition to yielding the required surface spectra (*i.e.*, apparent BRF and normalized radiance), yields supplementary information which can be used to verify the coherency of the atmospheric optical information derived from other sources or techniques. If the lowest altitudes are actually close to ground level this procedure is fortunately rather independent of the exact formulation used in the multi-altitude regression model. However even in such cases it is worthwhile formalizing the process so that the physical relevance of the extrapolation technique is not an issue in the validation of the atmospheric correction procedure.

The general equation (A-10) for the apparent BRF ($R^*(\tau_g)$) in the Appendix can be employed directly in a semi-empirical non-linear regression analysis to extract apparent surface BRFs as well as certain atmospheric parameters. From quasi-single scattering theory the total irradiance transmittance can be approximated by an exponential formulation (see for example, Miller and O'Neill, 1997):

where 'f', for irradiance transmission, is some fraction of $1/\mu_o$. Empirical studies with simulated radiative transfer data in a variety of turbid atmospheres (O'Neill and Freemantle, 1995) indicate that the diffuse transmission term and the atmospheric term can be approximated by expressions of the form:

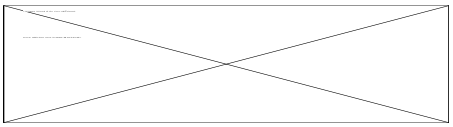

where e_1, e_2, a_1, and a_2 are empirical constants. Substituting equations (5), (6) and (7) into equation (A-10) yields:

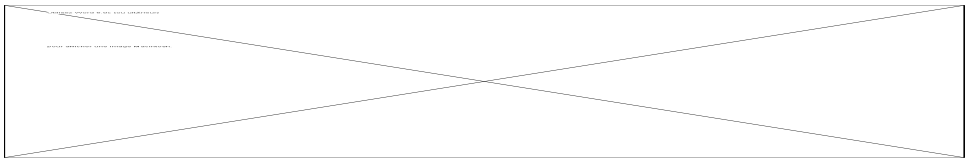

Molecular absorption via the multiplier defined in the Appendix (the transformation from (A-10) to (A-11)) was also incorporated into the empirical formulation defined above.

To a first order approximation the slope term $\upsilon(\tau_g)$ in equation (8b) can be replaced by an empirical constant and a simplified multi-altitude fit can then be applied to apparent BRF images to extract three height-independant fit parameters: the slope term $\upsilon(\lambda)$, the apparent surface BRF $R_{sur}^{*}(0, \lambda)$ and, assuming a fixed scale height atmosphere, the total aerosol optical depth from ground level to space. The quality of this simpler multi-altitude fit suffices if the only objective is to extrapolate multi-altitude apparent BRFs to the surface. Thus equation (8b) rather than (8a) can serve as a multi-spectral non-linear regression form to achieve reasonably fast regression procedures.

The slope term in equation (8b) requires careful interpretation. Its retrieved spectrum may contain (aside from gaseous absorption features) the preponderant influence of pure atmospheric scattering effects in the visible spectral region and, in the near infrared spectral region, strong environmental BRF effects if the background surface is very different from the target (forest surrounding a dark target for example). At the same time one expects the optical depth to be a slowly varying function of wavelength and indeed this provides a test of the physical validity of the multi-altitude regression. However, one must bear in mind that the quality of the fit parameters other than the apparent surface BRF is of secondary importance if the key objective is simply to achieve a best estimate of the apparent surface BRF.

METHODOLOGY

BOREAS Atmospheric Correction Validation Field Experiment

Location and timing

The BOREAS experiment was carried out over two specific study areas straddling the southern extreme of the Boreal forest near Prince Albert (PA) Saskatchewan (Southern Study Area or SSA) and the northern extreme near Thompson, Manitoba (Northern Study Area or NSA) during five major intensive field campaigns (IFCs) in 1994 (Sellers et al., 1995). The CASI sensor flew over all tower sites in both SSA and NSA during all five IFCs (Miller et al., 1995). The analysis in this paper is confined to July 24th of IFC-2 when atmospheric conditions were cloudless and reasonably free of the effects of the forest fire smoke which contaminated many other cloudless measuring days during IFC-2, particularly at the NSA (Miller and O'Neill, 1997).

Site descriptions

Two test sites in the SSA were chosen for the analysis of atmospheric correction procedures applied to CASI imagery. The first, a control calibration site was established at PA Airport as shown in Figure 1. This site contains a number of reference targets which were used to extract and/or validate the sensor BRF calibration and the atmospheric correction procedure. The figure shows a roll-corrected scene-recovery channel (src) acquired at 500 ft. above ground level. The key elements of this site included three 7.5 meter x 7.5 meter calibration panels of known BRF characteristics which were used to directly calibrate the CASI in terms of BRF. A large 50 meter x 125 meter asphalt tarmac reference target seen as the rectangular dark surface in the top half of the image was employed as a validation site for the BRF panel calibration. Target areas indicated as grass and runway were also used as homogeneous reference targets for validating the atmospheric corrections.

A second validation site was a flux tower site known as Old Black Spruce (OBS) located about 100 km to the northeast of the PA airport calibration site. This site, shown in Figure 2, contained a variety of forest classes (for which Black Spruce was the dominant species in poorly drained areas such as the tower site) in addition to more homogeneous targets over which we could apply the atmospheric correction procedure. The role of this site was to act as a benchmark atmospheric correction site in typical conditions of the boreal forest. It can be viewed as the final step of a validation process which encompassed controlled laboratory conditions for sensor radiance calibration, exterior but artificial calibration targets at PA airport for BRF calibration and validation and finally homogeneous natural targets at the OBS site for atmospheric correction validation.

CASI Imagery

The CASI acquires imagery in a number of user-definable modes which range between the extremes of full spatial mode (512 spatial pixels wide by 32 spectral bands) to variants of the full spectral mode (288 spectral bands by 39 spatial pixels). In spectral mode one wavelength channel is reserved for a full spatial presentation (the scene recovery or src channel) so that the coarser spatial resolution of the spectral mode can be superimposed on the highest spatial resolution of the instrument.

The intermediate spectral mode which we chose to employ in our analysis was configured for moderate spectral resolution across a choice of two spatial configurations: (i) a wide swath of 401 spatial pixels by 72 spectral bands with a 155 msec integration time and (ii) a narrow swath of 101 spatial pixels by 72 spectral bands with a 45 msec integration time. The instantaneous field of view (IFOV) of each pixel was 1.2 mrad while the aircraft velocity of approximately 60 meters/sec gave along track pixel dimensions equal to the projection of the IFOV on the ground plus 8.8 meters (for the 401 pixel mode) and the IFOV projection on the ground plus 2.6 meters (for the 101 pixel mode). The nominal spectral full width at half maximum (FWHM) of the 72 band mode was of 7.9 nm.

On the July 24th validation day, six multi-altitude images were acquired over the PA calibration site over a time period for which the solar zenith angle was 46 ± 2° (two at 500 ft., two at 2000 ft., and one each at 3000 ft. and 5500 ft. above ground level). Six images were acquired over the OBS site over a time period for which the solar zenith angle was 35 ± 1° (two at 500 ft., and one each at 2000 ft., 3000 ft., 5500 ft. and 8000 ft.). All images were roll-corrected and absolutely calibrated to radiance units as indicated below.

For every other line of acquired imagery, the downwelling irradiance probe data is transferred via fiber optic cable to the entrance slit of the CASI spectrometer such that it appears as a spatial pixel at the edge of the two dimensional CASI focal plane array. In this fashion it shares the spectral throughput characteristics of the radiance data and is well matched to this data whatever the state of absolute CASI spectral calibration. The post processing of this data includes a diffuser signal correction which normalizes attitude-induced variations of the downwelling irradiance back to an estimate of the digital level which would have been measured by a stable horizontal diffuser (Shepherd et al., 1995).

Ground Based Radiometry

Ground based validation spectra for the PA airport tarmac site were all acquired between July 21 and July 25 1994 using an ASD-PS2 based spectro-goniometer apparatus (Piekutowski et al., 1994). The BRF calibration of the 7.5 meter x 7.5 meter calibration panels described below in the calibration section was performed in the spring using the same spectro-goniometer apparatus.

Optical depth measurements were acquired using hand-held Sonotek sunphotometers (Smirnov et al., 1994) as well as fixed CIMEL sunphotometers at sites near Prince Albert airport and the OBS site. Continuous measurements throughout our July 24th validation day indicated that we could assume an aerosol optical depth value of 0.10 at 550 nm for both validation sites with a root mean square (rms) uncertainty of approximately +0.03. This rms figure was derived from instrumental intercomparisons and rms residual estimates from spatial/temporal interpolations. The fact that it is not symmetric about the nominal value simply reflects our choice of selecting and fixing a nominal value of aerosol optical depth prior to refinements in the determination of the aerosol optical depth variation. The effect of this choice, which is consistent with our approach of simplifying inputs to the atmospheric correction model, is analyzed below.

Atmospheric Correction Methodology

Our strategy in the atmospheric correction study was to validate a procedure which would be the simplest to carry out in an operational sense. This means that we began with a minimal input data set and employed default options built into the CAM5S model for the greater part of the model input requirements. Only where validation tests supported by physical arguments demonstrated that a particular parameter must be better defined would we offer an alternative logistical option for improving the accuracy of the atmospheric correction (in the sense of an alternative tradeoff option which the operational minded user might or might not implement in a large scale correction). Accordingly, the only parameter whose measured value was required as input was the aerosol optical depth across the whole atmosphere.

Atmospheric Correction Model

Atmospheric correction of all airborne data were performed using the CAM5S radiative transfer code. This code was derived from the 5S atmospheric radiative transfer model of Tanré et al.(1990) and the H5S code developed for airborne altitudes (Teillet et al., 1991). However in addition to this heritage it incorporates all the advantages of the recently released 6S model (Vermote et al., 1996) short of the time-consuming successive orders of scattering solution to the radiative transfer equation (O'Neill et al., 1996).

Inputs to the Atmospheric Corrections Methodology

With the above (minimum user input) strategy in mind, Table 1 describes the set of parameters employed as inputs to the atmospheric correction code which is run in "reverse" mode (extraction of apparent surface BRF given the at-altitude normalized radiance). Only those parameters or default choices in bold need to be specified by the user: the other parameters are for information only. The aerosol optical depth which is the only non-default parameter required in the model runs was derived from sunphotometer measurements as discussed above in the Ground Based Radiometry section.

CALIBRATION

Two independent calibration methodologies were used in our approach. The first (see the section "Radiance Calibration" below) was a more traditional absolute calibration where the CASI sensor was calibrated in the laboratory to achieve a linear transformation between scene grey levels and radiance. The second (see the section "BRF Calibration" below) was to employ reference BRF calibration panels to extract a CASI calibration factor $k(\lambda)$ between the ratio of scene digital numbers to downwelling irradiance digital numbers and the target BRF. In this latter case we seek to evaluate $k(\lambda)$ such that:

$$R_{sur}(\mu, \phi, -\mu_o, \phi_o+\pi) = k(\lambda) \frac{DN_L}{DN_{\mu_o E_o}} \qquad (9)$$

for a purely collimated solar beam. DN_L refers to digital number associated with the radiance of a given pixel in a given observation direction while $DN_{\mu_o E_o}$ refers to the digital number associated

(ideally) with a collimated downwelling solar irradiance which would be measured by the CASI downwelling sensor. It is noted that the DN_L values for images acquired with different integration times, as was the case between the PA airport and OBS sites, must be normalized by the integration time.

Radiance Calibration

The calibration procedure for extracting the linear transformation between CASI image digital numbers and radiance is described in Gray et al. (1997) (this issue). The conversion into normalized radiance was accomplished by integrating the values of extraterrestrial solar irradiance incorporated in CAM5S across the CASI bandwidths.

BRF calibration

Calibration panels

The BRFs of three calibration panels, nominally 4%, 16% and 32% were measured prior to the IFC-2 experiment by means of the spectro-goniometer apparatus as a function of a large variety of illumination and viewing conditions. These data were then fitted to the wavelength dependent parameters of the Coupled Surface-Atmosphere Reflectance (CSAR) model defined by Rahman et al. (1993). Given a lack of high frequency spectral variability, a small subset of the CSAR model parameters were then fitted to a second order spectral polynomial whose coefficients are given in the Appendix. This function was not chosen as the result of any intensive survey of BRF analytical models but rather as a reasonably simple analytical form which fitted the measured panel BRF to an acceptable accuracy and hence permitted extrapolations to geometries other than those in the original measurement database.

In general the procedure consisted of acquiring spectral measurements over numerous view and illumination conditions and over a sampling of positions at the edges of the panels as well as over a reference Spectralon reflectance panel (Piekutowski et al., 1994). These radiance measurements were performed under conditions of global irradiance and diffuse (solar occulted) irradiance conditions so that the latter could be subtracted from the former to achieve estimates of the true (direct beam) panel radiances. The calibration panel radiances were then normalized to the Spectralon reference radiance to estimate the BRF of each of the three panels for a grid of viewing and illumination geometries. The non Lambertian properties of the Spectralon reflectance panel itself were corrected for in the derivation of the three panel BRFs (ibid).

Extraction of $k(\lambda)$

For each of the three calibration panels the spectral ratio of radiance digital numbers (Fig. 4a) to irradiance digital numbers (Fig. 4b) were computed (Fig. 4c). The flight line data employed in the calculations (one at 500 ft. and two and 2000 ft.) were limited to those altitudes for which at least three CASI pixels could be accomodated within the area defined by any single panel. An altitude regression to achieve a surface representation of the ratio of radiance to irradiance sensor digital numbers over each calibration panel was performed in a manner similar to the methodology described

above for the apparent BRF. Because of the low altitudes over the calibration panels the results of the regression were virtually independent of the regression parameterization. This latter point is not surprising but nevertheless important since most of the parameters described in equation (8b) above could not be determined by the regression approach given that only two altitudes were available for the panels (two out of three of the parameters were fixed)

Once the surface level spectral ratios were obtained a set of three $k_i(\lambda)$ spectra (one for each panel) were computed from equation (9). These ratio spectra were then averaged to achieve a mean $k(\lambda)$ for all three panels. Figure 3(a) shows the mean $k(\lambda)$ factor derived from the BRF panel calibration and the spectral ratios of Figure 4(c) as well as the $k(\lambda)$ curve derived from the absolute calibration of the radiance and irradiance sensors (Freemantle, 1997). Because of problems in deriving the absolute irrradiance calibration factors the latter $k(\lambda)$ was normalized to the panel-calibration-derived $k(\lambda)$ at a particular channel in order to simply compare the forms of the two curves (see the Figure 3 caption). The good relative agreement between the forms of the spectral curves helps validate, in an independant fashion, the relative (panel) calibration procedure.

The relative difference between the $k(\lambda)$ factors for the three panels and their average ($|k_i(\lambda) - \langle k(\lambda) \rangle| / \langle k(\lambda) \rangle$) are plotted in Figure 3(b). This difference was less than 4% in the visible wavelengths and less than 10% for near infrared wavelengths.

Validation of $k(\lambda)$ over the tarmac reference target

A verification of the BRF calibration was carried out over the tarmac reference target of Figure 1. This target was sufficiently homogeneous and temporally stable to provide a good BRF reference and sufficiently large in extent to permit the extraction of an uniform pixel spectra at any altitude flown by the CASI. During the IFC-2 campaign the BRF of this target was intensively characterized by means of the ground-based spectro-goniometer apparatus applied to 16 different sampling stations across the western half of the tarmac surface. These data were assembled into a $R_{tarmac}(\theta_v, \theta_0, \phi_v - \phi_0)$ database and fitted with a simple analytical BRF function. Outliers were removed when they corresponded to field notes on specific anomalous reflection artifacts (the presence of small imbedded white stones in the tarmac for example were determined to be artifacts which would be averaged out by the larger field of view of the airborne sensor).

A Henyey-Greenstein type of BRF was found to provide a reasonably simple fit which accounted for all systematic variations (including a specular component) in the tarmac BRF. This specular component is not accounted for (and was never intended to be accounted for) in the Rahman model employed above for the panel BRF. The details of the model fit are given in the Appendix.

Having characterized the tarmac BRF via the ground-based spectro-goniometer apparatus the $R_{tarmac}^*(0)$ values derived from the altitude-regressed CASI measurements over the tarmac could then be validated. With reference to Figure 4, graph (d) shows the CASI upwelling scene digital numbers DN_L , (e) the downwelling CASI irradiance digital numbers (DN_E) and (f) the computed apparent BRF derived from the application of equation (9) to the ratio of (d) to (e). The higher red curve of Figure 4(f) shows the estimated $R_{tarmac}^*(0)$ derived from the multi-altitude regression technique discussed above while the smooth red curve directly underneath shows the results of the Henyey-Greenstein fit to the ground-based BRF measurements of the tarmac. Given that the rms residual error

bars about the latter spectra were $\leq .7\%$ for all wavelengths (c.f. Figure A1(b) for example) we note that the apparent BRF extrapolated to the surface (i.e. $R_{tarmac}^{*}(0)$)is within these rms bounds of precision.

Extraction of apparent surface BRF (ground-truth spectra) by multi-altitude regression over the tarmac

Figure 5 illustrates some results of the multi-altitude regression procedure for (a) the extraction of apparent surface BRF ($R_{tsr,ac}^{*}(0)$), (b) total aerosol optical depth and (c) the slope term υ (equation (8b)). One can note characteristic and important features for each of these three extracted parameters respectively: the $1/\lambda$ type of dependance for the total aerosol optical depth which indeed amounts to a preliminary validation of the methodology, the spectral smoothness of the $R_{sur}^{*}(0)$ spectra which is required for the ground target and finally the contribution of the environment in the near infra-red to the slope term as predicted in the theoretical discussion above. The total aerosol optical depth at 550 nm extracted by this method is comparable to the nominal sunphotometer-derived total aerosol optical depth which we employed in the atmospheric corrections procedure (0.14 versus 0.10 respectively). However, as stated above, the relative insensitivity of the $R_{tarmac}^{*}(0)$ extraction to the multi-altitude regression methodology is the essential feature of the procedure and we leave the discussion of the retrieval accuracy of these complementary optical parameters (aerosol optical depth and the slope term) to a future study.

ATMOSPHERIC CORRECTIONS: RESULTS AND DISCUSSION

Atmospheric Corrections over the PA reference Site

In this section we demonstrate the accuracy of the CAM5S based atmospheric correction procedure using the tarmac calibration target as well as the grass target and the bright runway target (see Figure 1). The particular choice of these latter targets from among a variety of possible targets in the PA airport images was motivated by our desire to validate the atmospheric correction procedure over a wide range of target signatures but more importantly by the need to ensure that the validation analysis was carried out only over those targets for which we could be sure that the radiance variance due to spatial misregistration of targets between altitudes was of significantly less importance than the atmospherically-induced variance which we wished to analyze. Practically this meant that the radiance variance in the neighbourhood of selected targets should be small for a given altitude.

Figure 6 shows the CAM5S atmospheric correction procedure applied to all three validation targets. The red curves represent the (apparent) surface BRF derived from the multi-altitude apparent BRF regression procedure and is our best estimate of the true (apparent) surface BRF ($R_{sur}^{*}(0)$). The blue curve is the high-altitude apparent BRF which is derived from the CASI $k(\lambda)$ calibration and which is the spectra being corrected. The atmospherically-corrected BRF (black curve) is the standard (ρ_c) inverse mode output of CAM5S where the input spectra to CAM5S was actually normalized radiance (ρ^{*}). The latter ρ_c curves show the atmospheric correction achieved by ignoring any differential environmental effect between the target BRF and the

environmental BRF (labelled $\rho_e = \rho_c$) while the green curves account for a differential environmental effect by using the nominal vegetation standard of CAM5S as the environmental BRF (labelled $\rho_e \neq \rho_c$).

We note that the normalized radiance ρ^* is not shown in the figures since this quantity cannot be compared directly with the apparent surface BRF whose validation is our ultimate goal (cannot be compared directly in the very real sense that ρ^* does not tend towards ρ_c as the altitude decreases). The CAM5S output of ρ_c is shown without modification since, within the confines of the Lambertian approximation option of CAM5S, this quantity is directly comparable with the apparent surface BRF or $R_{sur}^*(0)$. It is also important to understand that both the absolute (radiance) and relative $k(\lambda)$ calibrations are being tested here: ρ^* is derived from the CASI radiance normalized to published extraterrestrial solar irradiance data (a database incorporated in CAM5S) integrated across the CASI bands while the other two spectra of Figure 6 result from the $k(\lambda)$ calibration.

In the first (tarmac) target one can observe a distinct improvement after atmospheric corrections in the visible spectral region while the correction actually makes matters worse in the near infrared region. This apparent anomaly is rectified by approximately accounting for the differential environmental effect. In fact, the near infrared ($\rho_e \neq \rho_c$) curve is significantly improved relative to the ($\rho_e = \rho_c$) curve (see Figure 6(a)). The result of not accounting for a differential environmental effect translates into an overestimation of the importance of attenuation effects and a subsequent over-correction. In the curve which accounts for the differential environmental effect the enhanced scattering contribution of the environment is accounted for and the attenuation over-correction is appropriately counterbalanced.

The persistance of absorption artifacts in the corrected curves, is probably due to slight shifts in the spectral calibration of the CASI sensor which manifest themselves as very sensitive indicators of spectral phase shifts between the position of true narrow absorption features and their analogue in the nominal CASI spectrum (Williams et al., 1992).

In the case of the second (runway) target the atmospheric correction procedure does not significantly change the level of agreement relative to the true apparent surface BRF in the visible spectral region because we are faced with an equilibrium phenomenom wherein scattering effects approximately balance out attenuation effects (O'Neill et al., 1995). In the near infrared spectral region the attenuation effect is overemphasized as it was in the corresponding curve for the tarmac target because the scattering contribution of the vegetation environment is neglected. When this effect is accounted for (green curve) one notes a significant improvement in the near infrared atmospheric correction accompanied by a marginal improvement in the visible spectral region.

In the third validation curve (grass target) one observes an improvement in the visible spectral region after correction while in the near infrared region an over-correction is noted. When the environmental effect is accounted for there is little change in the visible since the environment is in any case close to the target BRF while some slight improvement can be noted in the near infrared. As pointed out below this type of improvement where we employ a standard environmental BRF must be taken with a grain of salt because the utilisation of such an input and its associated uncertainty necessarily limits our claims to an improved correction.

Atmospheric Corrections over the OBS (Old Black Spruce) Site

The second phase of the atmospheric correction validation involved the application of the CAM5S correction procedure to selected targets near and at the OBS benchmark site. Five targets were chosen in this phase of the validation exercise (two lake targets, a forest target, a cut-over and a sand target. The analysis technique presented in Figure 7 is identical to Figure 6 inasmuch as we have presented the apparent surface BRF, the uncorrected apparent BRF at altitude and the CAM5S corrected spectrum. Again the black-coloured spectral curves represent the correction without accounting for a differential environmental effect while this effect has been accounted for in the green-coloured spectral curves.

One can observe the significant improvement brought about by the atmospheric correction procedure for the first water target (White Swan Lake). The surface BRF signature shows a spectral dependency which is typical of a reasonably clear and deep lake far removed from the shore. The rather large discrepancy remaining after accounting for the environmental effect is due to another standardized input to the CAM5S model: a zero target size. Such an input simplifies the correction methodology, as is our goal, but clearly is unsatisfactory when the target size is a few kilometers as was the case here. Inputting a correct average target size into the model (and thereby increasing the logistical complexity of the methodology) had the expected effect of making the atmospheric correction insensitive to the inclusion of the differential environmental effect (closer to the $\rho_e = \rho_c$ curve).

In the second water target (White Gull Lake) the improvement is significant although less spectacular than for White Swan Lake. This lake appears to be considerably more turbid than the latter as can be observed in the magnitude and shape of the surface BRF spectrum. However we note that spectral peak near 700 nm is probably more indicative of the presence of submerged vegetation (Borstad et al., 1985) rather than what could be attributed to extremely chlorophyll rich waters.

In the third (Black Spruce stand) target one may observe an improvement after atmospheric corrections in the visible region while the near infrared correction induces a slight decrease in accuracy relative to the surface BRF. The inclusion of the differential environmental effect improves the comparison. However one must keep in mind that the environmental surface BRF is a canned standard of CAM5S and there is no reason to expect that the vegetation standard of the code is actually closer to the background environment than one obtains by assuming the background surface BRF is identical to the target (*i.e.*, the assumption for the black-coloured $\rho_e = \rho_c$ curves).

The fourth target (cut-over) shows once again an improvement in the visible portion of the spectrum while there is no improvement in the near infrared region. The inclusion of the environmental effect in this case improves the comparison in the visible region and marginally degrades the comparison in the near infrared region. Finally the fifth target (beach sand) shows a distinct improvement after atmospheric correction in the visible region and a degradation in the near infrared region. Accounting for the environmental effect improves the comparison in the visible region and degrades the comparison in the near infrared region.

Discussion of the Calibration and Atmospheric corrections results and the Coherence of the Radiative Transfer Physics in general.

Table 2 summarizes all the atmospheric correction results for the ensemble of sampling points presented in Figures 6 and 7. These pairs of numbers (unbracketed and bracketed) represent the relative errors as well as the absolute differences both expressed as percentage between the atmospherically uncorrected or atmospherically corrected BRFs relative to our best estimate of the apparent surface BRF ($R^*_{true}(0)$) and subsequently averaged over the visible spectral region (left half of the tables) and over the near infrared part of the spectral region (right half of the tables). Mathematically they can be approximated by the integrals:

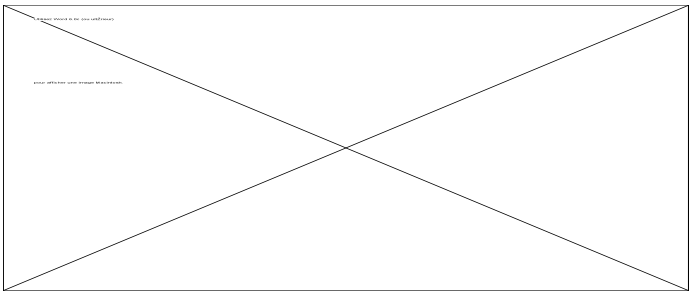

where $[\lambda_a, \lambda_b]$ = [480 nm - 710 nm] for the visible spectral region and [710 nm - 913 nm] for the near infrared region. The choice of 710 nm as a dividing wavelength corresponds approximately to the vegetation red shoulder inflection point and, given the importance of vegetation spectra to our analysis, seemed to us a natural division point for the error averages. The columns marked ($\rho_e = \rho_c$) represent atmospheric corrections which do not account for the differential environmental effect while the columns marked ($\rho_e \neq \rho_c$) indicate that a differential environmental effect has been included (using the standard CAM5S vegetation environment).

The table clearly indicates quantitatively what was stated or implied in the preceding section, that there are significant improvements in the estimated surface BRF (i) when the actual surface BRF is weak, (ii) when the environmental effect is applied for a weak target in the presence of a strong background (in particular for the near infrared case of a weakly reflecting target surrounded by vegetation) and (iii) in the radiative equilibrium case (scattering approximately balanced by attenuation for strongly reflecting targets) little improvement occurs (or is needed).

In terms of absolute apparent BRF differences (equation (10b)) the best standard corrections (including the use of a standard vegetation environment) yielded average after-correction differences over the eight validation targets of 0.6% in the visible region and 1.4% in the near infrared region compared to pre-correction differences of 1.6% and 1.1% respectively (if recognition of target size is included for the environmental effect over the lakes the post correction numbers drop to 0.5% and 1.1% respectively). The analogous relative differences (equation 10(a)) were post-correction values of 24% in the visible and 122% in the near infrared versus pre-correction values of 61% and 59%). The post-correction values drop to 11% and 27% when target size information was available (the relative numbers are clearly dominated by the lake corrections since these BRFs were so small). In the near infrared case an improvement brought about by an atmospheric correction is only evident for weakly reflecting (non vegetation) targets where scattering effects predominate over attenuation effects.

With respect to the nominal input value of aerosol optical depth it will be recalled that a lower limit of $\tau_a(550\ \text{nm.}) = 0.1$ was used (where the estimated rms departure from this lower limit was

+ 0.03). Calculations performed for a sampling of targets showed that the corresponding uncertainty in the extracted apparent surface BRF was: $\Delta R^*_{sur}(0) < \Delta\tau_a/10$ or less than 0.3% absolute uncertainty in the apparent surface BRF. This value although not insignificant does not alter any of the qualitative observations presented above.

Table 3 presents a set of results which are entirely analogous to those of Table 2 except that the atmospheric corrections were driven by apparent BRF rather than normalized radiance. This means that the model had been modified to accept CASI-specific apparent BRFs (from the $k(\lambda)$ calibration) and to directly correct these spectra to apparent surface BRF. Since these results are of about the same quality in terms of the error tables we conclude that this redundancy further validates the calibration and atmospheric correction procedures.

CONCLUSIONS

An atmospheric correction procedure using a variant of the 5S radiative transfer model (CAM5S) and based on standard model inputs (aside from the aerosol optical depth) yielded significant improvements in the surface BRF estimated from normalized radiance when the target was weakly reflecting (such as for the Boreal forest in the visible spectral region). Significant improvements were also noted when a default environmental background was used to correct for the case where a weakly reflecting target was subject to the environmental influence of a strong reflecting background (such as for a vegetation background in the near infrared. Assuming a knowledge of the local aerosol optical depth and some apriori information on the type of environment surrounding each validation site the average absolute differences between the uncorrected and corrected apparent BRFs and the ground truth apparent BRFs were 1.6% versus 0.6% respectively in the visible spectral region and 1.1% versus 1.1% respectively in the near infrared region

A new relative BRF calibration technique which employs the ratio of upwelling radiance signals to downwelling irradiance signals and calibrated reference panels of known BRF was carried out and validated over a test target of known BRF. This technique when combined with multi-altitude imagery yields estimates of apparent surface BRF which can be employed as "ground truth" data to validate atmospheric corrections of high and mid altitude data. This BRF validation data must necessarily be more relevant than traditional spot sampling on the ground since it is acquired for sampling geometries which are much closer to the observing conditions of the sensor whose imagery is to be atmospherically corrected. A coherent methodology for the extrapolation of the at-altitude apparent BRFs to the surface BRF was introduced. Such extrapolations are appropriately insensitive to the exact methodology when the lowest altitudes are close to ground level but become more critical when this is not the case.

It is worth emphasizing that the procedures which we employed incorporated two distinct calibration methodologies: an absolute calibration using laboratory radiance standards and the relative BRF calibration carried out entirely in the field. The two methods are to a large extent

complementary and do much to increase the understanding of the radiative transfer mechanisms involved and hence the confidence which one can attribute to the extracted values of apparent surface BRF.

A supplementary validation was performed in which the the atmospheric correction model was modified in order to receive, process and correct at-sensor apparent BRF rather than normalized radiance. These results showed comparable accuracies to the atmospheric correction procedure which employed normalized radiance as input and thus further confirmed our confidence in the total BRF calibration and atmospheric correction methodology. What was not demonstrated in this study but which nonetheless merits commentary is that the methodology of at-sensor BRF acquisition and processing offers particular advantages over traditional radiance based airborne remote sensing: (i) the atmospheric correction of imagery in less than ideal atmospheric conditions with uniform cloud above the sensor (e.g. high altitude cirrus) is much more readily accomodated and (ii) the normalization of radiance imagery by an optical signal proportional to downwelling irradiance and subject to the same radiometric and spectrometric influences (the same optical train) removes or minimizes all common sources of undesired variance (spectral offsets for example) and as such is a powerful argument for BRF normalization.

In general the atmospheric correction results can be improved with more precise estimates of correction model inputs at the cost of increased complexity in the atmospheric correction methodology. A fair amount of research effort within the remote sensing community is nonetheless dedicated to finding image-based methodologies for estimating the second order correction inputs (any input other than the aerosol optical depth) in addition to image derived estimates of the aerosol optical depth. This effort should be guided by a centralist strategy of calibration and validation which demonstrates the accuracy vs methodological complexity tradeoffs inherent in the adoption of a given technique for a given input parameter.

ACKNOWLEDGEMENTS

The authors would like to acknowledge the financial support of the Natural Science and Engineering Research Council in terms of the individual research grants of O'Neill, Royer and Miller as well as a collaborative research grant for the BOREAS project. Contributions of financial aid or resource support from CESL (Canadian Expert Support Lab), CCRS (Canada Center for Remote Sensing), FCAR (Fonds pour la Formation de Chercheurs et l'Aide à la Recherche) and ISTS (Institute for Space and Terrestrial Science) are also gratefully acknowledged. Individual contributions from Patrick Cliche, Minh Nguyen and Thomas Piekutowski of CARTEL, Lawrence Gray and Paul Shepherd of ISTS and Gladys Hann-O'Neill were essential to the realization of this work.

APPENDIX

In this appendix we complete the theoretical discussion presented in O'Neill et al. (1995) in order to obtain explicit apparent BRF and apparent normalized radiance expressions for the non Lambertian solution employed in 6S and in our combined 6S/5S version (CAM5S).

Surface BRFs

From equation (19a) of O'Neill et al. (1995) one can express the apparent BRF of all surface-derived terms as:

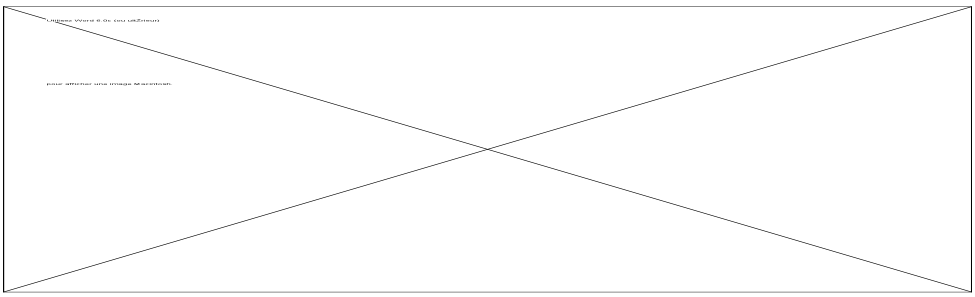

where ρ is the average bi-hemispherical reflectance of pixels surrounding the target pixel (known as the environmental bi-hemispherical reflectance in the case of a single pixel or zero radius target but in general represents an average of the target bi-hemispherical reflectance when the target is of finite size plus the bi-hemispherical reflectance of non target pixels). Converting equation (A-1) to normalized radiance yields:

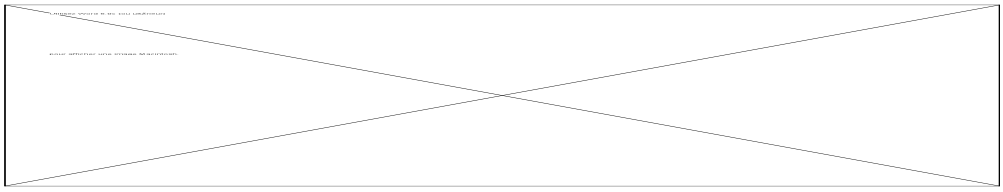

We note that if the total downwelling irradiance given by equation (3) above is subdivided into its diffuse and direct components:

then the diffuse downwelling irradiance is necessarily:

where the absence of a surface reflectance argument (ρ) in the argument list of E_{dif} means the calculation is performed in a zero reflecting atmosphere. Note that the direct term enters as a diffuse term which has gone through one reflection by the surface and the atmosphere. Dividing by $\mu_o E_o$ one can express this relation in terms of diffuse and direct transmissions in a non-

reflecting atmosphere (the functions typically employed in the 5S and 6S radiative transfer models):

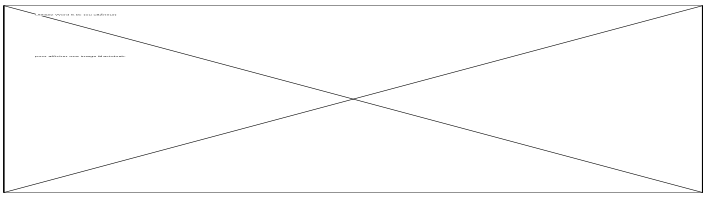

The third term of the surface-derived normalized radiance above (equation (A-2)) assumes a Lambertian reflectance. If instead we proceed from first principles, the transmission term of equation (14b) from O'Neill et al. (1995) is:

$$\pi L_{env}(\tau, \mu, \phi) = \frac{1}{\pi} \int_0^{2\pi} \int_0^1 T_{atm}(\tau_o - \tau; \mu, \phi, \mu', \phi') \, \mu' \, L_g(\mu', \phi') \, d\mu' \, d\phi',$$

where the surface radiance from equation (4) of the same reference is:

$$\pi L_g(\mu, \phi, -\mu_o, \phi_o+\pi) = \overline{R}_{env}(\mu, \phi) E_{dif} + R_{env}(\mu, \phi, -\mu_o, \phi_o+\pi) E_{dir}.$$

and where E_{dir} and E_{dif} are direct and total diffuse irradiance at the surface (optical depth $\tau = \tau_o$ from the top of the atmosphere or $\tau_g = \tau_o - \tau = 0$ from the surface). R_{env} denotes a surface BRF average for all pixels surrounding the target pixel. Substituting this expression into the transmission term of equation (14b) of O'Neill et al., 1995 yields:

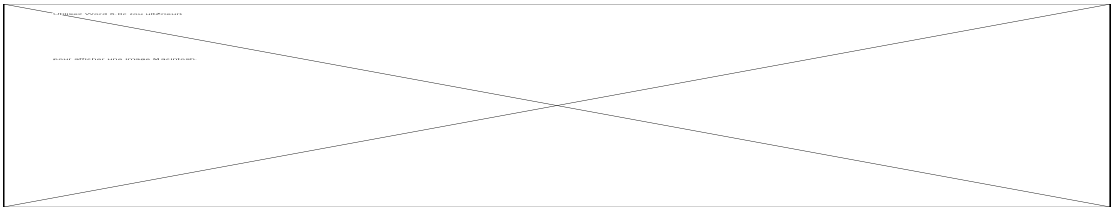

If the transmission is replaced by the average transmission over all upwelling angles (μ', ϕ') then:

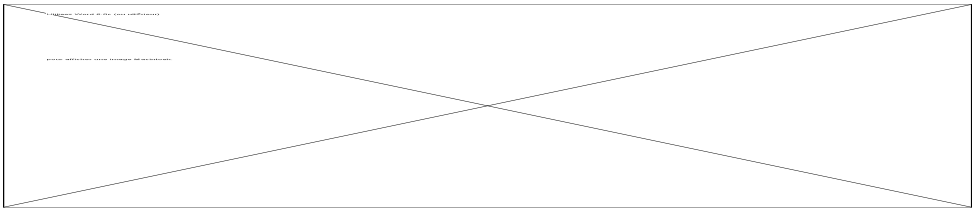

or hence:

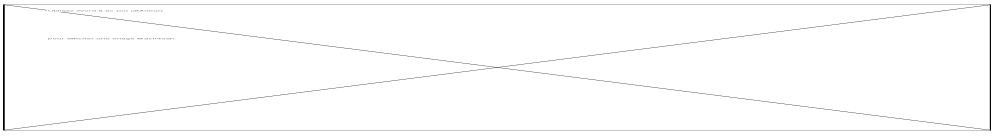

where the prime indicates integration over the upwelling hemisphere. The normalized radiance represented by equation (A-7b) can be associated with the diffuse transmission of diffuse (sky) and direct (solar) photons reflected by the environment surrounding the target. Thus the complete expression for the surface-derived terms takes on the form:

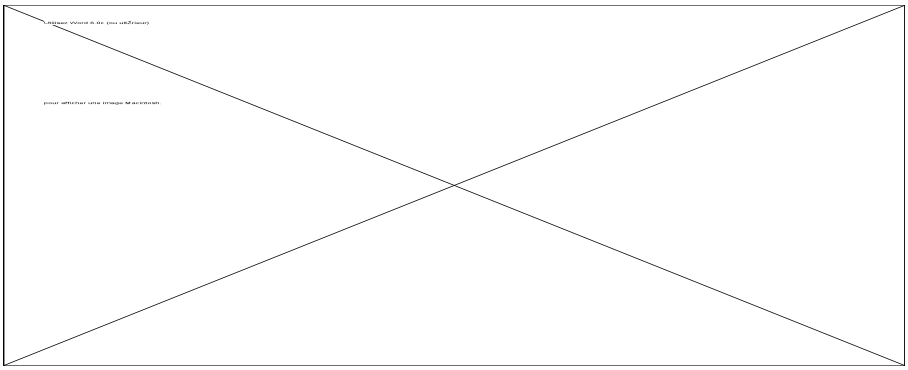

The target and environment expressions can be recast in terms of the most direct quantity obtained from an atmospheric correction, the apparent surface BRF:

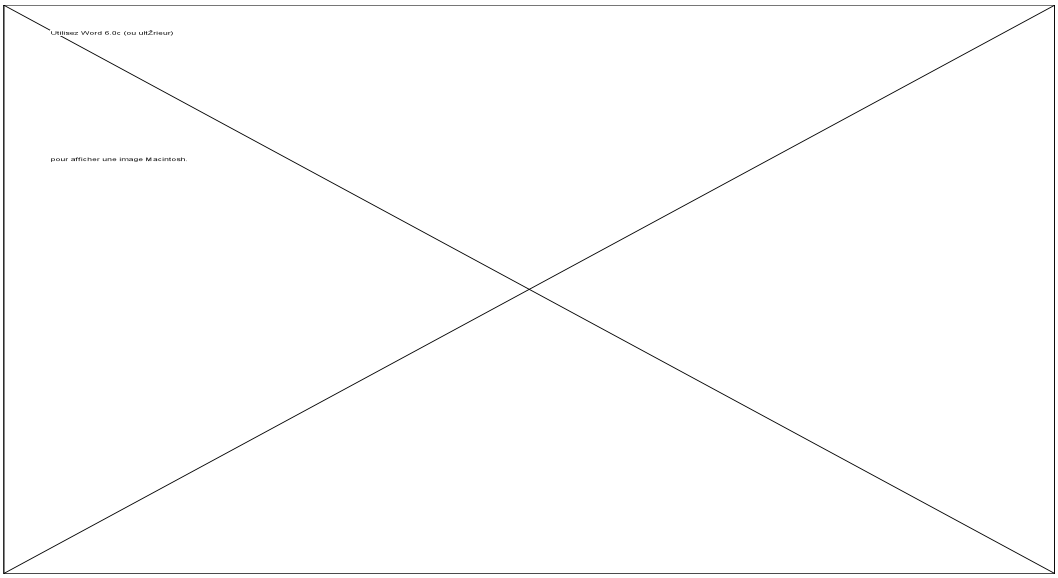

The apparent surface target BRF ($R_{sur}^{*}(0,\mu,\phi,-\mu_o,\phi_o+\pi)$) is, aside from a final step of decoupling the directional-directional BRF, the quantity sought in atmospheric corrections.

The generalized expression for normalized radiance at airborne levels can be sudivided into the target component and environmental components defined above and a pure atmospheric component (ibid). Employing equation (A-8) above and clumping all pure atmospheric terms of the generalized expression (19a) in O'Neill et al. (1995) into ρ_{atm} yields:

where the transmission factors of the third term are approximately independent of surface reflectance effects. Multiplying through by $\mu_o E_o / E_{tot}(\tau_g) = 1/T_{tot}(\tau_g)$ yields the apparent BRF equivalent of equation (A-9):

$$R^*(\tau_g) = R^*_{env}(\tau_g) + R^*_{atm}(\tau_g) + R^*_{sur}(\tau_g)$$

$$= \overline{R}^*_{env}(0)\, h(\tau_g)\, T_{atm}(\tau_g; \mu, \phi) + R^*_{atm}(\tau_g) + R^*_{sur}(0)\, h(\tau_g)\, e^{-\tau_g/\mu} \qquad (A-10)$$

$$\text{where } h(\tau_g) = \frac{T_{tot}(0)}{T_{tot}(\tau_g)}$$

Effects of Molecular Absorption

The expressions above are perfectly general and implicitly incorporate atmospheric molecular absorption. However, as is often done in atmospheric radiative transfer where molecular absorption processes are largely independant of scattering processes, one can to a reasonable approximation, separate out the molecular absorption contributions in terms of a multiplicative transmission factor. A further approximation which is employed in models such as 5S and 6S is to presume that diffuse irradiances, can at least as far as estimating the transmission factors is concerned, be represented by line of sight transmission factors about the solar direction for downwelling radiation and about the target to sensor direction for upwelling radiation.

This approximation means that all unitless radiative ratios such as r(0) and the angularily-averaged BRFs above are independent of molecular absorption and we need only account for the transmission between the aircraft and the ground and the ground and the aircraft. The following transformations accordingly yield a generalized expression which incorporates the molecular absorption approximate:

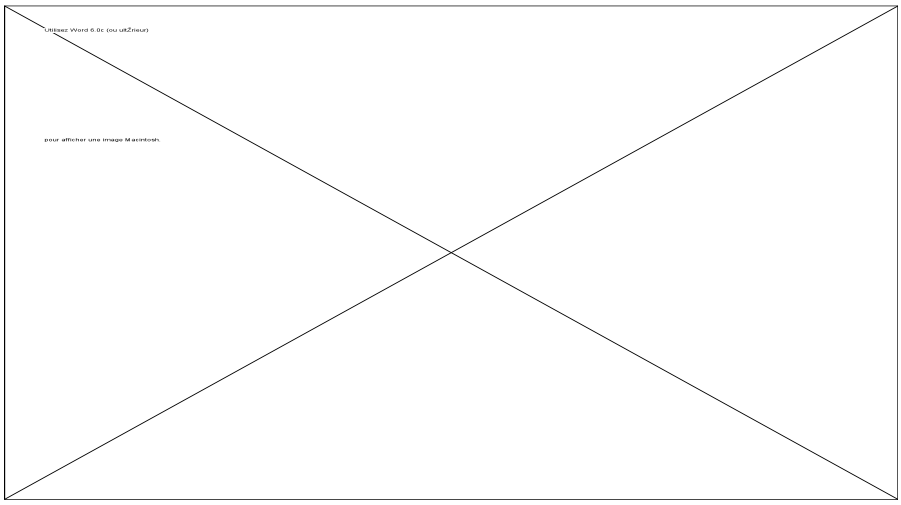

where $t_{gas}(z, \mu)$ is the molecular transmission from ground level to altitude z or from altitude z to ground level along the zenith direction represented by μ.

BRF of calibration panels

BRF measurements for the 7.5 meter x 7.5 meter calibration panels were fitted to the BRF model of Rahman et al. (1993). All four Rahman parameters were in turn fitted to a spectral polynomial whose form and coefficients are given in the table below.

Table A-1: Fit parameters to the CSAR function:
$x = a_0 + a_1\lambda + a_1\lambda^2$ where $x = \rho_0, \delta, \kappa$ or Θ

	4% Panel			16% Panel			32% Panel		
	a_0	a_1	a_2	a_0	a_1	a_2	a_0	a_1	a_2
ρ_0	0.0279	0.0285	0.0219	0.0411	0.1571	-0.0854	0.0810	0.2640	-0.1383
δ	0.1392	1.3911	-0.9551	-0.0023	2.1289	-1.3950	0.1506	2.0680	-1.0947
κ	0.5347	0.9153	-0.4511	0.6067	0.4645	-0.1934	0.6668	0.3861	-0.1710
Θ	0.0206	-0.4416	0.0816	0.2543	-0.5405	0.2285	0.2265	-0.3992	0.1658

PA tarmac BRF

The form of the Henyey-Greenstein function employed to fit the PA tarmac BRF was taken as:

where χ the scattering angle between the reflected radiance and the specular direction is given by the usual expression:

The azimuth difference $\phi - \phi_0$ is equal to π for the specular direction. The values for K and g are given in Table A-2 for four of the nominal spectro-goniometer (ASD PS-2) wavelengths.

Table A-2. Spectral variation of the Henyey-Greenstein fit coefficients

λ (nm)	g	K
499.66	0.206	0.034
600.64	0.181	0.039
700.19	0.177	0.041
799.74	0.180	0.043

The fit for 500 nm (499.66 nm nominal ASD wavelength) as well as the residual to the fit are shown in Fig. A-1 as a function of the scattering angle χ.

In the next step the derived Henyey-Greenstein parameters and the associated BRF residuals were extrapolated across wavelength using the four initial wavelengths above in a second degree polynomial:

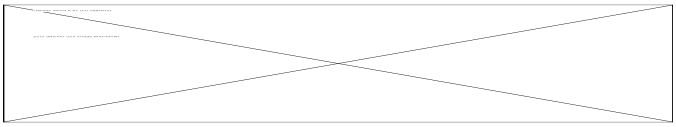

with λ in units of nm. A linear fit to the original BRF residuals gives:

$$<\delta R_{sur}^{2}>^{0.5} = 0.00515 + 4.9996 \times 10^{-6} \lambda$$

where the rms average is across all measurements (a single rms residual per wavelength channel was computed for all stations and all measuring days and then this quantity was extrapolated across wavelength).

REFERENCES

Borstad G.A., H.R. Edel, J.F.R. Gower, and A.B. Hollinger. 1985. "Analysis of Test and Flight Data from the Fluorescence Line Imager ", Canadian Special Publication of Fisheries and Aquatic Sciences, Department of Fisheries and Oceans, Ottawa.

Fraser R.S., R.A. Ferrare, and Y.J. Kaufman. 1992. "Algorithms for Atmospheric Corrections of Aircraft and Satellite Imagery", *International Journal of Remote Sensing.,* Vol. 13, pp. 541-557.

Freemantle, J. R. 1997. Personal communication,

Gray L., P. Shepherd, J. Freemantle, J. Miller, J. Harron and C. Hersom. 1997. "Calibration of the CASI Airborne Imaging Spectrometer for BOREAS", *Canadian Journal of Remote Sensing*, this issue.

Kaufman Y.J., and D. Tanré. 1993. "Strategy for Direct and Indirect Methods for Correcting the Aerosol Effect on Remote Sensing: From AVHRR to EOS-MOSDIS", *Remote Sensing of Environment,* Vol. 55, pp. 65-79.

Miller J.R., J.R. Freemantle, P.R. Shepherd, L. Gray, N.T. O'Neill, A. Royer and E. Senese. 1995. Deployment of CASI to Meet the Needs of BOREAS Science, *Proceedings of the 17th Canadian Remote Sensing Symposium*, Saskatoon Saskatchewan, pp. 169-175.

Miller J.R. and N.T. O'Neill. 1997. Multi-Altitude Airborne Observations of the Insolation Effects of Forest Fire Smoke Aerosols at BOREAS: Estimates of Aerosol Optical Parameters, accepted for publication in the *Journal of Geophysical Research*.

O'Neill N.T., A. Royer, Q. F. Xu, P. M. Teillet. 1997. "Retrieval of Atmospheric Optical Parameters from Airborne Flux Measurements: Application to the Atmospheric Correction of Imagery", *Applied Optics*, Vol. 36:3, 662-674.

O'Neill N.T., A. Royer and M.N. Nguyen. 1996. Scientific and Technical Report on the Development of a Modified Version of the H5S code which incorporates major features of the 6S Code, CARTEL internal report CARTEL-1996-020, Sherbrooke, Québec, 62 pp.

O'Neill N.T., and J.R. Freemantle. 1995. "Radiative Transfer Benchmark Results for Airborne Multi-Altitude Radiance and Irradiance Computations", CARTEL internal report CARTEL-1995-020, 19 pp.

O'Neill N.T., J.R. Miller and J.R. Freemantle. 1995. "Atmospheric Correction of Airborne BRF to Yield Surface BRF: Nomenclature, Theory & Methods", *Canadian Journal of Remote Sensing,* Special Issue on Airborne Remote Sensing, Vol. 21:3, 309-327.

Piekutowski T., A.T. Hoang, and N.T. O'Neill. 1994. "Calibration of CCRS Reflectance Panels", Report MIFUCAM-T1-CCRP, Sherbrooke, Québec, 47 pp.

Rahman H., B. Pinty, and M.M. Verstraete. 1993. "Coupled surface-atmosphere reflectance (CSAR) model: 2) Semiempirical surface model usable with NOAA Advanced Very High Resolution Data", *Journal of Geophysical Research,* 98(D11):20791-20801.

Sellers P., F. Hall, H. Margolis, B. Kelly, D. Baldocchi, G. Den Hartog, J. Cihlar, M.G. Ryan, B. Goodison, P. Crill, K.J. Ranson, D. Lettenmaier, and D.E. Wickland. 1995. "The Boreal Ecosystem-Atmosphere Study (BOREAS): An Overview and Early Results from the 1994 Field Year", *Bulletin of the American Meteorological Society*, Vol. 76, No. 9, pp. 1549-1577.

Shepherd P.R., N.T. O'Neill, and T. Piekutowski. 1995. "Analysis of Downwelling Upwelling Diffuser Probe Data to Determine At-Sensor Irradiance Fluxes", Proceedings of the 17th Canadian Symposium on Remote Sensing, Canadian Remote Sensing Society, Saskatoon, Saskatchewan.

Smirnov A.V., A. Royer, N.T. O'Neill and A.Tarussov. 1994. "A Study of the Link between Synoptical Air Mass and Atmospheric Optical Parameters", *Journal of Geophysical Research*, Vol. 99, N D10, pp. 20967-20982.

Teillet P.M., and R.P. Santer. 1991. Terrain Elevation and Sensor Altitude Dependance in a Semi-Analytical Atmospheric Code, Canadian Journal of Remote Sensing, Vol. 17, No. 1, pp. 36-44.

Tanré D., C. Deroo, P. Duhaut, P.M. Herman, J.J. Morcrette, J. Perbos, and P.Y. Deschamps. 1986. "Description of a Computer Code to Simulate the Satellite Signal in the Solar Spectrum: the 5S Code", *International Journal of Remote Sensing ,* Vol. 11, pp. 659-668.

Vermote E., D. Tanré, J.L. Deuze, M. Herman, and J.J. Morcrette. 1996. Second Simulation of the Satellite Signal in the Solar Spectrum (6S), 6S User's Guide, Version 1, Laboratoire d'Otique Atmosphérique, Lille, France, 214 pp.

Williams D., A. Royer, N.T. O'Neill, S. Achal, and G. Weale. 1992. "Reflectance Extractionfrom CASI Spectra using Radiative Transfer Simulations and a Rooftop Irradiance Collector, *Canadian Journal of Remote Sensing*, Vol. 18, No. 4, pp. 251-261.

Zagolski F. and J.P. Gastellu-Etchegorry. 1995. "Atmospheric Corrections of AVIRIS Images with a Procedure Based on the Inversion of the 5S Model", *International Journal of Remote Sensing.,* Vol. 16(16), pp. 3115-3146.

GLOSSARY OF SYMBOLS (see O'Neill et al., 1995 for details)

Symbol	Description
apparent BRF	The adjective "apparent" stems from the fact that this quantity is a surface BRF which has been modified by the presence of an atmosphere. In airborne cases there is an added complication in that the downwelling irradiance which is employed to normalize the upwelling radiance is not a collimated beam as is required for a pure BRF (see also the more formal definition of $R^*(\tau_g; \mu, \phi, -\mu_o, \phi_o+\pi)$ below)
BRF	Bidirectional Reflectance Factor. A pure BRF is characterized by a source of illumination which is collimated: therefore one can never directly measure a pure BRF within the earth's atmosphere (see also O'Neill et al., 1995).
DN	digital number
E_o	extraterrestrial solar irradiance on a plane perpendicular to the solar rays.
$E_{dif}(\tau_g, \mu_o, \rho)$	downwelling diffuse irradiance at optical depth.
$E_{dif}(\tau_g, \mu_o)$	downwelling diffuse irradiance at optical depth τ_g for the pure atmospheric case (non reflecting surface).
$E_{dir}(\tau_g, \mu_o)$	downwelling direct irradiance ($= \mu_o E_o \exp[- \tau / \mu_o]$) at optical depth τ_g.
$E_{tot}(\tau_g, \mu_o, \rho)$	downwelling irradiance at optical depth τ_g ($= E_{dir}(\tau_g, \mu_o) + E_{dif}(\tau_g, \mu_o, \rho)$)
$E_{tot}(\tau_g, \mu_o, 0)$	downwelling irradiance at optical depth τ_g for the pure atmospheric case (non reflecting surface). Also written as $E_{tot}(\tau_g, \mu_o)$ $E_{tot}(\tau_g, \mu_o, 0) = E_{dir}(\tau_g, \mu_o) + E_{dif}(\tau_g, \mu_o)$
$\phi_o, \phi_o + \pi$	solar azimuth, $\phi_o + \pi$ implies a ray directed away the sun (opposite azimuth to the sun).
$\phi, \phi + \pi$	azimuth of radiation direction, $\phi + \pi$ implies a ray from a source of azimuth ϕ or towards an observer of azimuth ϕ.

$k(\lambda)$	factor for transforming the ratio of upwelling radiance digital levels to downwelling irradiance digital levels into an apparent BRF (c.f . equation (9) in the text).
$L(\tau_g, \mu, \phi)$	radiance at optical depth τ_g, ray zenith cosine μ, and ray azimuth ϕ.
μ_o, $-\mu_o$	cosine of the solar zenith angle (θ_o), negative sign implies a ray from the sun in the opposite direction to the sun.
μ, $-\mu$	zenith angle cosine of radiation direction (θ), negative sign implies a ray from a source of zenith angle θ (cosine μ) or towards an observer at zenith angle θ (cosine μ).
ρ	Bi-hemispherical reflectance averaged over the total ground surface surrounding the target (weighted mean of ρ_e and ρ_c).
ρ_e	Environmental (bi-hemispherical) reflectance averaged across the total surface outside of the target. The subscript "env" is reserved for an environment which consists of the total environment surrounding the target pixel (which may be only one pixel of a larger target surface).
ρ_c	Bi-hemispherical reflectance averaged over the target surface (which may be larger than a pixel). The subscript (which in order to be consistant with the notation in this article would be "sur") is the subscript employed in the 5S/6S models. If one assumes a Lambertian surface target reflectance (a standard assumption) then $\rho_c = R^*_{sur}(0)$.
$\rho^*(\tau_g, \mu, \phi, -\mu_o, \phi_o+\pi)$	general at-sensor normalized radiance = $\pi\, L(\tau_g, \mu, \phi) / \mu_o E_o$
$R^*(\tau_g, \mu, \phi, -\mu_o, \phi_o+\pi)$	general apparent at-sensor BRF = $\pi\, L(\tau_g, \mu, \phi) / E_{tot}(\tau_g, \mu_o, \rho)$. Also written as $R^*(\tau_g)$ for short.

$R^*(\tau_g; \mu, \phi, -\mu_o, \phi_o+\pi)$ apparent BRF at altitude z or surface to sensor optical depth τ_g (see equation (1a))

$R^*_x(\tau_g; \mu, \phi, -\mu_o, \phi_o+\pi)$ apparent atmospheric: (x = atm) or environmental (x = env) BRF

$R_{sur}^*(0, \mu, \phi, -\mu_o, \phi_o+\pi)$ apparent surface BRF of a given target
$= \pi L_{sur}(0, \mu, \phi) / E_{tot}(0, \mu_o, \rho)$.
Also written as $R_{sur}^*(0)$ for short. This apparent BRF is the result of an atmospheric correction of $R^*(\tau_g)$. The "apparent" label derives from the fact that the quantity is a transformation of the true surface BRF. It can be written as (O'Neill et al., 1995) :

$$R_{sur}^*(0, \mu, \phi, -\mu_o, \phi_o+ \pi) = \bar{R}_{sur}(\mu, \phi)\, r(0) + R_{sur}(\mu, \phi, -\mu_o, \phi_o + \pi)\, [1 - r(0)]$$

$R_{sur}(\mu, \phi, -\mu_o, \phi_o+\pi)$ true target BRF

$\bar{R}_{sur}(\mu, \phi)$ true target BRF averaged over the downwelling hemisphere (c.f. equation (5)) of O'Neill et al., 1995)

$R_{env}(\mu, \phi, -\mu_o, \phi_o+\pi)$ BRF spatial average about the target pixel (environment)

$\rho^*_x(\tau_g; \mu, \phi, -\mu_o, \phi_o+\pi)$ apparent atmospheric (x = atm) or environmental (x = env) normalized radiance.

$r(\tau_g)$ ratio of diffuse downwelling irradiance to total downwelling irradiance at optical depth τ_g (altitude z).

$s(\tau_g)$ spherical albedo: hemispherical-hemispherical reflectance of the atmosphere above the layer of optical depth τ_g

τ optical depth (aerosol scattering + absorption and molecular scattering from outside the atmosphere to altitude z).

τ_g optical depth (aerosol scattering + absorption and molecular scattering from ground level to altitude z).

τ_o total atmospheric optical depth ($\tau_o = \tau_g + \tau$)

θ_o solar zenith angle ($= \cos^{-1}\mu_o$)

$T_{tot}(\tau_g, \mu_o, \rho)$	Diffuse + direction transmission at optical depth τ_g (= $t_{dir}(\tau_g, \mu_o, \rho) + t_{dif}(\tau_g, \mu_o)$). At ground level ($\tau_g = 0$) these quantities are also written without the argument τ_g in the text (see equations following equations (A - 8) in the Appendix).
$T_{atm}(\tau_g; \mu, \phi, -\mu_o, \phi_o+\pi)$	diffuse transmission factor for the atmospheric layer of optical thickness τ_g
$t_{dif}(\mu_o, \rho)$, $t_{dif}(\mu_o)$	diffuse transmission in an atmosphere of average surface bi-hemisphereical reflectance ρ and zero respectively (see equation (A - 5) in the Appendix)
$t_{dir}(\mu_o)$	direct solar transmission (see equation (A - 5) in the Appendix)
$t_{gas}(z, \mu)$	molecular transmission from ground level to altitude z or from altitude z to ground level along the zenith direction represented by μ.
z	altitude above ground level.